

THE NEW GRADIENT RECOVERY AND EXTERNAL DOMAIN ERROR ESTIMATORS: EXTENSION TO 2-D ELASTOSTATICS BEM

Ariosto B. Jorge*, Gabriel O. Ribeiro[†], and Timothy S. Fisher**

*Department of Mathematics and Computer Sciences,
UNIFEI – Federal University at Itajubá,
Av BPS, 1303, Itajubá, MG, Brazil - CEP 37500-000.
Email: ariosto.b.jorge@unifei.edu.br

[†]Department of Structural Engineering,
UFMG – Federal University of Minas Gerais,
Av do Contorno, 842 - 2o andar, Belo Horizonte, MG, Brazil - CEP 30110-060.

**School of Mechanical Engineering,
Purdue University, West Lafayette, IN 49707, USA.

Keywords: Boundary Element Methods (BEM), Error Estimators, Gradient Recovery, Elastostatics

Abstract. *Two new error estimators for the BEM in 2-D potential problems were recently presented by the authors. This work extends these two error estimators for 2-D elastostatics problems. The first approach involves a local error estimator based on a gradient recovery procedure in which the error function is based on differences between smoothed and non-smoothed rates of change of boundary variables in the local tangential direction. The second approach is associated with the external problem formulation and gives both local and global measures of the error, depending on a choice of the external evaluation point. These approaches are post-processing procedures. Both estimators show consistency with mesh refinement and give similar qualitative results. The error estimator using the gradient recovery approach presents a more general characteristic as its formulation does not rely on an “optimal” choice of an external parameter, such as in the case of the external domain error estimator. Also, the external domain error estimator can be used only for domains in which an exterior region exists.*

1 INTRODUCTION

This work extends two new error estimator approaches in boundary element methods (BEM) for 2-D elastostatics problems. These error estimator approaches were recently presented by the authors for 2-D potential problems.¹ The extension of these error estimators for a problem with a different integral formulation highlights their generality of use.

Error estimators based on residuals and error norms, similar to the approaches available in the finite element method (FEM), have been used for symmetric BEM formulations, but the error estimators literature is scarce for the collocation BEM formulation. Reviews for error estimation and adaptivity methods for BEM can be found in Liapis² and Kita and Kamiya^{3,4}

The two local error estimator approaches presented in this work can be used for both Galerkin and collocation BEM formulations. The first approach involves a gradient recovery procedure, wherein the smoothed or recovered functions are rates of change of the boundary variables in the local tangential direction. The gradient recovery approach is commonly used in the finite element method⁵ and considers the evaluation of the gradient of the field variable in global coordinates, with continuous derivatives of this field variable in fixed global directions. On the other hand, in the BEM the variables of interest are written in local coordinates. The displacements are continuous throughout the boundary, while the tractions and the tangential derivatives of the boundary variables may be discontinuous, such as at points where the boundary is not smooth or where the boundary conditions are discontinuous.

The second error estimator approach is associated with an external problem formulation and gives both a local and a global measure of the error depending on the external point where the equation is applied. Denda⁶ presented an error estimator for elasticity based on the strain energy in the exterior region. In the current work, the error estimator is obtained using directly the error in the displacements and in the stresses obtained from the exterior problem. The displacements and the stresses should vanish at points located in the exterior of a closed domain. Nonzero values indicate errors. If the external evaluation point is near the boundary, the influence of the nearby boundary elements in the error estimate will be dominant, and the error information assumes a local characteristic. To eliminate any influence of the choice of the global directions on the values of the stress error estimates, the stresses at the exterior point are first combined into stress invariants, the mean stress and the octahedral stress, before any error information is evaluated.

In the present work, the two estimates are computed for two 2-D elastostatics problems, of which one contains a singularity. A comparison is made between global and local error estimates. The error consistency with mesh refinement is also compared.

2 THE GRADIENT RECOVERY FOR ELASTOSTATICS BEM

The concept of recovery of derivatives for error estimation originated with finite element methods, in which error indicators were derived from derivatives of the computed finite element solution. A procedure to smooth the gradient to compute these derivatives with good accuracy is called gradient recovery.⁵ The derivatives are evaluated from a weighted average of element derivatives surrounding a node. The weighting factors are the element areas.

This post-processing approach to estimate error from gradient recovery was adapted by the authors to 2-D potential BEM problems in Ref.¹ An important feature in this procedure when applied to FEM is that the derivatives of the field variables (displacements) are taken with respect to a global coordinate system. Thus, not only are the field variables continuous at the domain nodes, but also the smoothed gradient vectors in a general elastostatics problem are continuous. On the other hand, when the gradient recovery procedure is applied to BEM, the tangential and normal directions are written in local coordinates at a boundary point, and discontinuities in the tangential derivatives need to be allowed in both the original and the recovered tangential derivatives of the density fields (boundary displacements and tractions).

To write a system of equations similar to the one obtained with the FEM procedure, continuity would be required for the derivatives of the densities. The approach adopted in Ref.¹ and extended in this work is to introduce double nodes at all the discontinuous points, such as the corner nodes on the boundary. Elements with zero length connect these double nodes, so that no local or global contribution for the error from these fictitious elements is incurred. The concept of double nodes to account for discontinuities in the tractions when obtaining the boundary solution is well known in the BEM literature⁷ but is not used in this work. The double nodes introduced here originate from discontinuities in the values of the tangential derivatives of the densities at corner nodes in the *post-processing* algorithm to obtain the element errors and not from the original BEM procedure to evaluate the boundary solution.

The basic boundary integral equation for the elastostatics problem,⁸ gives the displacement $u_j(x)$ as a function of boundary integrals. This displacement-BIE, can be written, for an homogeneous domain Ω as:

$$C_{ji}(p)u_i(p) = \int_{\partial\Omega} \Psi_{ji}(p, Q)t_i(Q)dS(Q) - \int_{\partial\Omega} T_{ji}^\psi(p, Q)u_i(Q)dS(Q) \quad (1)$$

where $Q \in \partial\Omega$. The functions Ψ_{ji} and T_{ji}^ψ are associated with fundamental solutions of the Navier equation. The integrals in Eq. 1 provide a constraining equation for the boundary variables when evaluated for $p \in \partial\Omega$, which is called the collocation point.

Four different densities must be considered when writing a boundary integral equation for 2-D elastostatics: the two components of the displacements, $u_1 = u$ and $u_2 = v$, and the two components of the tractions, $t_1 = SG$ and $t_2 = TAU$. In this work, recovery of the tangential derivatives of each density is made independently, so that separate element

error information is obtained for each of the four boundary densities. In a later step, the element residuals are combined into element errors that contain information from the recovery of the tangential derivatives of all four densities.

In what follows, a boundary density is denoted by ϕ ($\phi = u, v, SG$ or TAU) and its tangential derivative by $\partial\phi/\partial s$. The solution at any point inside the element (e) is $\phi^{(e)}(\xi) = [N] \{\phi\}^{(e)} = \sum_{i=1}^m N_i(\xi)\phi_i^{(e)}$, where ξ is the intrinsic coordinate and m is the number of element nodes corresponding to the polynomial interpolation being used. Taking derivatives with respect to the intrinsic coordinate gives

$$\left(\frac{d\phi}{ds}\right)^{(e)} = \left(\frac{d\phi}{d\xi}\right)^{(e)} \left(\frac{d\xi}{ds}\right)^{(e)}, \text{ where } \left(\frac{d\phi}{d\xi}\right)^{(e)} = \left[\frac{dN}{d\xi}\right] \{\phi\}^{(e)} \quad (2)$$

and $J(\xi, s) = (d\xi/ds)^{(e)}$ is the Jacobian of the transformation between the real element (with coordinate s) and the standard element (with the intrinsic coordinate ξ).

These derivatives can be written with polynomial shape functions one degree higher as

$$\left(\frac{d\phi}{ds}\right)^{(e)*} = [N] \left\{\frac{d\phi}{ds}\right\}^{(e)*} \quad (3)$$

where $\{d\phi/ds\}^{(e)*}$ is the set of nodal values of the corresponding derivatives, equivalent in a local averaging sense, to the original ones, $\{d\phi/ds\}^{(e)}$. The element equivalence is enforced by requiring that both formulations for the derivatives give same element integrals, defined by

$$I_\phi^{(e)} = \int_{S^{(e)}} \{N\} \left(\frac{d\phi}{ds}\right)^{(e)*} ds = \int_{S^{(e)}} \{N\} \left(\frac{d\phi}{d\xi}\right)^{(e)} J(\xi, s) ds \quad (4)$$

where the integration is performed on $S^{(e)}$, which is the element length in 2-D or the element area in 3-D. If the element under integration is now written as $ds = J(s, \xi)d\xi$, where $J(s, \xi) = ds/d\xi = 1/J(\xi, s)$, all terms in the integrands are only functions of the intrinsic variable ξ , and all element integrations are performed for $\xi \in [-1, 1]$, for the usual Lagrangian interpolating functions.

The element equations in Eq. 4 are then assembled for the entire boundary S , leading to an expanded system of equations that includes the original elements and the new zero-length elements at the double nodes.

A simple procedure is implemented in this work to account automatically for these new zero-length elements when assembling the system of equations. The procedure consists of three steps. In the first step, a test is performed at each node i , for discontinuities in the tractions or in the normal unit vector between the elements that share the node. A corner locator variable is set to a value of one wherever a corner is located or a discontinuity in traction exists.

The second step is to renumber the current nodes and elements to include the zero-length elements at the located “corner” nodes. A new augmented connectivity matrix is thus created relating node/element numbering, including the added zero-length elements. With this procedure, single values for the tractions and for the tangential derivatives of both the displacements and the tractions can be assigned to each node in the augmented system. An assembled system of equations is thus obtained from which the vectors of smoothed nodal derivatives $\{\partial\phi/\partial s\}^{(e)}$ can be obtained in this augmented system. The system matrix for the coefficients of the recovered or smoothed quantities is not singular and admits an inverse after assembling all elements.

The third step is to evaluate the element errors still in the augmented system and then renumber backwards the nodes/elements to their original numbering, by excluding the zero-length elements, so that only the error information of the original elements is retained.

The recovery of all four densities ($\phi = u, v, SG$ or TAU) is implemented in this work so that error estimators are obtained separately from the smoothed tangential derivatives of the displacements and of the tractions, and also a combined error estimator is obtained when the individual contributions from the tangential derivatives of the various densities are added. A scaling parameter is introduced so that the individual contributions are scaled before being added.

Implementation of the tangential derivative recovery for linear elements

The gradient recovery procedure for the elastostatics problem follows directly from the similar procedure for the potential problem as established in Ref.¹ The recovery of the derivatives of the potential and the flux in¹ is substituted by the recovery of the derivatives of the two components of the displacement, and of the two components of the tractions.

The procedure has two steps. In the first step all the element smoothed derivatives of the displacements and of the tractions are obtained from the solution of the four separate system of equations, assembled from the element equations for each density. In a second step an element residual is defined for the non-zero length elements by combining the residuals from the displacements and the tractions. Finally, the element error is obtained from this residual.

The first step, consisting of the recovery of the tangential derivative for each density ($\phi = u, v, SG$ or TAU), is now detailed. A standard linear element has two end nodes with corresponding shape functions $N_1(\xi) = (1 - \xi)/2$ and $N_2(\xi) = (1 + \xi)/2$ for $\xi \in [-1, 1]$. The shape function derivatives are $N_1'(\xi) = -1/2$ and $N_2'(\xi) = 1/2$. The Jacobian for this 1-D straight element is $J(\xi, s) = \partial\xi/\partial s = 2/L^{(e)}$, where $L^{(e)}$ is the length of the boundary element (e). The element of integration is $dS^{(e)} = (L^{(e)}/2)d\xi$. The original (non-smoothed) and the recovered (smoothed, denoted by $*$) tangential derivatives of the

density are written for the element (e) as

$$\left(\frac{\partial\phi}{\partial s}\right)^{(e)}(\xi) = \left[\frac{\partial N}{\partial\xi}\right]\frac{\partial\xi}{\partial s}\{\phi\}^{(e)} = \frac{2}{L^{(e)}}[N_1'(\xi) \quad N_2'(\xi)]\begin{Bmatrix}\phi_1^{(e)} \\ \phi_2^{(e)}\end{Bmatrix} \quad (5)$$

$$\left(\frac{\partial\phi}{\partial s}\right)^{(e)*}(\xi) = [N_1(\xi) \quad N_2(\xi)]\begin{Bmatrix}\frac{\partial\phi_1}{\partial s}^{(e)*} \\ \frac{\partial\phi_2}{\partial s}^{(e)*}\end{Bmatrix} \quad (6)$$

so that the equivalence relation of Eq. 4 can be enforced. After substituting the shape functions and performing the integrals, the element equivalence equation is obtained as

$$\frac{L^{(e)}}{3}\begin{bmatrix}2 & 1 \\ 1 & 2\end{bmatrix}\begin{Bmatrix}\frac{\partial\phi_1}{\partial s}^{(e)*} \\ \frac{\partial\phi_2}{\partial s}^{(e)*}\end{Bmatrix} = \begin{bmatrix}-1 & 1 \\ -1 & 1\end{bmatrix}\begin{Bmatrix}\phi_1^{(e)} \\ \phi_2^{(e)}\end{Bmatrix} \quad (7)$$

Now all element matrices given by Eq. 7 can be assembled for a particular mesh with N elements. By solving the assembled system of equations, the vector of nodal values for the smoothed tangential derivatives of the density $\{\partial\phi/\partial s\}^{(e)*}$ are obtained. Because the assembled matrices are sparse, special methods can be used to solve the assembled system.⁹ The vector of element interpolations for the original non-zero elements is now obtained from Eq. 3 as

$$\left(\frac{\partial\phi}{\partial s}(\xi)\right)^{(e)*} = N_1(\xi)\frac{\partial\phi_1}{\partial s}^{(e)*} + N_2(\xi)\frac{\partial\phi_2}{\partial s}^{(e)*} \quad (8)$$

where the index (e) is taken, so that only the interpolations for the non-zero elements are retained. The residuals $r_{\phi^{(e)}}^2$ are now evaluated for each of these elements as the square of the differences between the smoothed solution obtained in Eq. 8 and the original non-smoothed solution obtained from Eq. 2.

$$r_{\phi^{(e)}}^2(\xi) = \left[\left(\frac{\partial\phi}{\partial s}(\xi)\right)^{(e)*} - \left(\frac{\partial\phi}{\partial s}(\xi)\right)^{(e)}\right]^2 \quad (9)$$

The element errors $E_{\phi^{(e)}}$, the average error $E_{\phi_{AVE}}$ and the normalized element errors $E_{\phi_{norm}^{(e)}}$ are

$$E_{\phi^{(e)}} = \left[\int_{-1}^1 r_{\phi^{(e)}}^2(\xi)d\xi\right]^{\frac{1}{2}}\frac{L^{(e)}}{L_{total}} \quad E_{\phi_{AVE}} = \frac{1}{N}\sum_{(e)}E_{\phi^{(e)}} \quad E_{\phi_{norm}^{(e)}} = \frac{E_{\phi^{(e)}}}{E_{\phi_{AVE}}} \quad (10)$$

where L_{total} is the length of the entire boundary. The element errors $E_{\phi^{(e)}}$ are weighted by the relative element length to account for element sizes while evaluating the average error $E_{\phi_{AVE}}$. The average error is a measure of the global error and is used to obtain the

normalized element errors $E_{\phi_{norm}^{(e)}}$. The normalized local error indicator could be used in an adaptive mesh refinement procedure.

The above procedure is performed four times to obtain the smoothed tangential derivatives of the various densities and the corresponding element residuals, leading to the various individual contributions for the element errors. In this work, the tangential derivatives of the displacements are multiplied by G (the shear modulus) to minimize possible numerical inaccuracies involving small numbers. A more general local error estimator is obtained when combining the individual contributions of the four densities. The non-normalized element errors are combined by means of adding after scaling.

In this work, two separate scaling factors for the tangential derivatives of the displacements (combined) and the tractions (combined) were constructed by evaluating average values of these tangential derivatives in each non-zero length element and adding these element contributions to the scaling factor, after weighting the element contribution by the relative element length. Each element contribution to the scaling factor is an average of the element tangential derivative of the density evaluated using the smoothed and the non-smoothed variables. The element contribution to the scaling factor for the tangential derivative of each density is obtained as follows.

$$SF_{\phi^{(e)}} = \frac{\left[\left(\frac{d\phi}{ds} \right)_{AVE}^{(e)*} \right]^2 + \left[\left(\frac{d\phi}{ds} \right)_{AVE}^{(e)} \right]^2}{2} \frac{L^{(e)}}{L_{total}} \quad (11)$$

where the element average using the smoothed variables is given by

$$\left(\frac{d\phi}{ds} \right)_{AVE}^{(e)*} = \left[\frac{1}{2} \quad \frac{1}{2} \right] \left\{ \frac{d\phi_1}{ds} \right. \\ \left. \frac{d\phi_2}{ds} \right\}^{(e)*} \quad (12)$$

and the element average using the non-smoothed variables is given by

$$\left(\frac{d\phi}{ds} \right)_{AVE}^{(e)} = \frac{1}{L^{(e)}} \begin{bmatrix} -1 & 1 \end{bmatrix} \left\{ \phi_1 \right. \\ \left. \phi_2 \right\}^{(e)} \quad (13)$$

Separate scaling factors for the tangential derivative of the densities are obtained as

$$SF_{\phi} = \frac{1}{N} \left[\sum_{(e)} SF_{\phi^{(e)}} \right]^{\frac{1}{2}} \quad (14)$$

for $\phi = u, v, SG$ and TAU . The scaling factor for the tangential derivatives of the displacements (SF_D) is obtained as an average of the separate scaling factors for u and v : $SF_D = (SF_u + SF_v)/2$. Similarly, the scaling factor for the tangential derivatives of the tractions (SF_T) is obtained as an average of the separate scaling factors for SG and

TAU : $SF_T = SF_{SG} + SF_{TAU}$. The element error with combined contributions from the tangential derivatives of both the displacements and the tractions is obtained as

$$E_{GR:D+T}^{(e)} = \frac{E_u^{(e)} + E_v^{(e)}}{SF_D} + \frac{E_{SG}^{(e)} + E_{TAU}^{(e)}}{SF_T} \quad (15)$$

The obtained local error $E_{GR:D+T}^{(e)}$ with combined scaled contributions of the tangential displacement derivatives and the tractions is non-dimensional. The average error $E_{D+T_{AVE}}^{(e)}$ and the normalized element errors $E_{D+T_{norm}}^{(e)}$ are obtained by replacing ϕ by $D + T$ in the second and third equations of Eq. 10.

3 THE EXTERNAL DOMAIN APPROACH FOR ELASTOSTATICS BEM

The external domain error estimator approach is based on the difference between two equivalent formulations. The exact solution for one integral representation a problem satisfies any other possible different integral representation of the same problem. When a numerical solution is found for one formulation, this solution can be substituted into the discretized form (with same discretization) of the other possible formulation. Because numerical solutions are not exact, the identities in the discretized form of this second formulation will not be satisfied. The difference is a measure of the discretization error of both formulations.

The external domain approach uses the fact that, for a closed domain, the exterior boundary integral representations for both the displacements and the stresses equal zero in the elastostatics problem. Thus, any difference from zero can be related to the discretization error. Because fundamental solutions are functions of the distance between source and field points, one representation in which the exterior point is very close to the boundary might give a different error measure than the case in which the point is far away from the boundary. If different exterior points are considered, several external formulations may be obtained. The error measure is sensitive to the external point position for non-trivial problems.

To implement the procedure, first a numerical solution at the boundary is obtained for the discretized mesh using a collocation BEM formulation. This boundary solution is then substituted into the discretized integral representations for the interior displacements and stresses, and finally these displacements (u and v) and stresses (σ_x , σ_y and τ_{xy}) are evaluated at an exterior point $y^{(e)}$ in a close vicinity to a boundary element (e). An external error estimator for the total displacement ($Ext : D$) is constructed as

$$E_{Ext:D}^{(e)} = \left[u \left(y^{(e)} \right)^2 + v \left(y^{(e)} \right)^2 \right]^{1/2} \quad (16)$$

External error estimators can be defined from the stresses at the exterior point, as well. To eliminate any influence of the choice of global directions on the values of the stress error estimates, the stresses at the exterior point are combined into stress invariants to

obtain error estimators. Two external errors estimators are adopted in this work: the octahedral stress ($Ext : T$) and the mean stress ($Ext : M$), given by

$$E_{Ext:T}^{(e)} = \frac{\sqrt{2}}{3} [\sigma_x^2 - \sigma_x\sigma_y + \sigma_y^2 + 3\tau_{xy}^2]^{1/2} \quad E_{Ext:M}^{(e)} = (\sigma_x + \sigma_y)/2 \quad (17)$$

with σ_x , σ_y and τ_{xy} evaluated at the exterior point $y^{(e)}$. Naturally, if the numerical boundary solution is exact, all external error estimators are zero.

The exterior evaluation point $y^{(e)}$ is located at a distance from the boundary (the distance from the exterior point to the closest point on the boundary) that is a fraction α of the size of the nearest boundary element (e). This distance is measured from the element center in the normal direction to the element at this point. In this work, numerical experiments are done with various values of α in order to evaluate the most appropriate location for the external point y . The closer the external point to the boundary, the more “local” the error information is. On the other hand, if the external point is too close to the boundary, numerical errors may appear due to quasi-singularities.

The external domain error estimators can also be combined to obtain a more general error estimator ($Ext : D+T+M$) with error information from both external displacements and stresses. The individual contributions for element error are also scaled before adding, with the scaling factors defined as the average boundary total displacement $(v^2 + v^2)^{1/2}$ and total traction $(SG^2 + TAU^2)^{1/2}$, respectively.

In Section 4, the element errors $E_{Ext}^{(e)}$ for various values of α are compared. Comparisons are also made between $E_{Ext}^{(e)}$ and $E_{GR}^{(e)}$ to show the consistency of the local information given by these estimates with mesh refinement. We note that the external domain error estimator can be used only for domains in which an exterior region exists. For example, if using a traction-BIE without a multiregion approach for the case of a crack embedded in an infinite elastic body, no exterior region could be defined in which the evaluation point would be at a finite distance from the boundary. In this case, the external domain error estimator could not be used, while the gradient recovery approach can always be used, for closed or open boundaries, and for finite or infinite domains.

4 IMPLEMENTATION OF THE PROPOSED ERROR ESTIMATORS

Two numerical examples of elastostatics are performed to demonstrate the implementation of the two proposed error estimators. The first problem involves a plate with a central crack. Due to symmetry, one-quarter of the cracked plate is modeled. The crack tip creates a discontinuity in the normal traction at the smooth point in the intersection between the two different types of boundary conditions. When discretizing the boundary, numerical errors are expected at the elements near this singular point, as the boundary solution will not be able to reproduce exactly the singular traction on one side of the crack tip.

The second problem involves an axisymmetric pressurized pipe with curved boundary segments. Also, this problem presents two special features, due to the geometry and

boundary conditions. The first feature is that in the boundary segments corresponding to radial directions, only the tangential derivatives (which are, in this case, radial derivatives) of the densities change. The second feature is that on the circular arcs of the pipe boundary the exact tractions are constant, so their tangential derivatives are zero. The boundary elements (linear elements, in this study) do not preserve the circular arcs, thus local errors are expected on the approximate boundary.

All BEM results were obtained with the code SERBA presented in Paris and Cañas⁷ with 12-point Gaussian integration. This code uses linear elements, but the error estimator procedures proposed in this work can be adapted to use any degree in the element polynomial interpolants.

The two problems have the tangential traction TAU prescribed as equal to zero everywhere, thus this traction is not discontinuous. On the other hand, the normal traction SG is discontinuous at all corners due to the discontinuity in the normal direction to the adjacent elements. Also, a discontinuity in the normal traction exists at the singular point (the crack tip) in the first problem. Local errors are expected in a vicinity of these "corners" as the numerical code evaluates the unknown discontinuous normal traction.

4.1 The cracked plate problem

This well known problem consists of a rectangular plate with a central crack. Due to the symmetry in the geometry and in the boundary conditions, only one-quarter of the cracked plate is modeled. Figure 1(a) shows the problem geometry and boundary conditions. The elastic modulus is $E = 2.1 \times 10^6$ units and Poisson's ratio is $\nu = 0.25$. A singularity in the normal traction is created at the crack tip, point O in Fig. 1(a).

Four meshes are considered to compare the error estimators. Figure 1(b) shows the initial coarse mesh with 78 elements. Knowing the existence of a singularity at the crack tip, two types of mesh refinement are adopted. r -refinement is performed by rearranging the nodal positions so that the mesh density increases on both sides of the boundary region near the crack tip. This rearrangement is performed without changing the overall number of nodes. Figure 2(a) shows the r -refined mesh with 78 elements. Mesh refinement (h -refinement) is also performed (both for the original and r -refined meshes) by dividing each element by two. The two meshes with 156 elements (original and r -refined) follow the same idea and are not shown.

All element matrices given by Eq. 7 can be assembled for the various meshes. For all cases, the number of elements in the expanded system of equations includes the original elements plus four zero-length elements that were added at the boundary corners and one zero-length element that was added at the crack tip, which is treated as a "corner" because the normal traction is discontinuous at this singular point.

By solving the assembled system of equations, the vector of nodal values for the smoothed tangential derivatives of the densities is obtained. The residuals are evaluated using Eq. 9, and the element errors $E_{GR}^{(e)}$ are obtained using Eq. 10 and compared with the local element errors $E_{EXT}^{(e)}$, obtained using Eqs. 16 and 17.

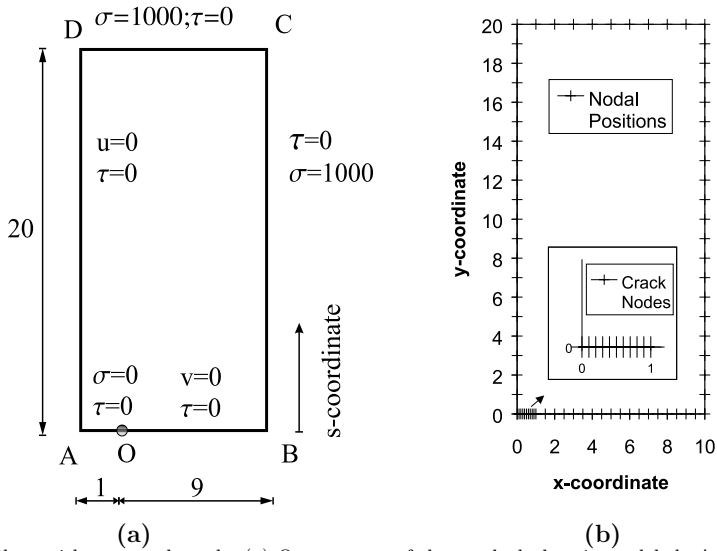


Figure 1: Plate with a central crack. (a) One-quarter of the cracked plate is modeled. A singularity in the normal traction is created at the crack tip (point O). (b) Coarse mesh (initial): 78 elements.

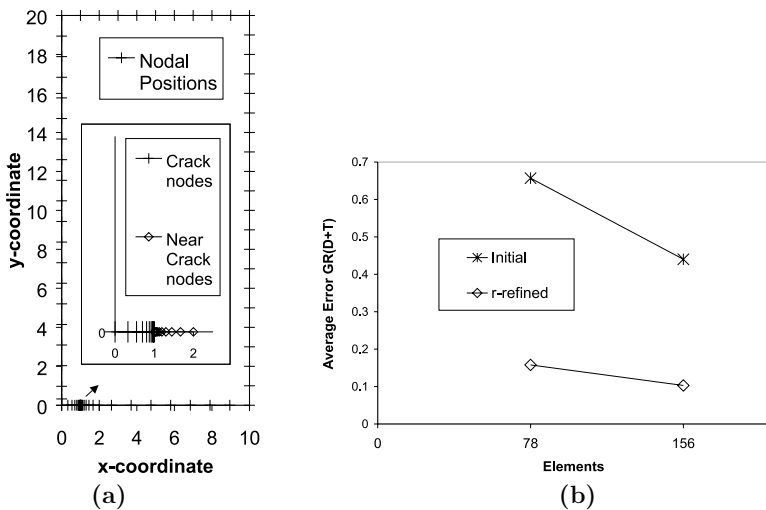


Figure 2: Cracked plate problem. (a) Coarse mesh (r -refined): 78 elements. Small elements are concentrated near the crack tip. (b) Average (global) error estimators for the Gradient recovery (GR:D+T) procedure. Similar behavior (not shown) for the errors from the external domain approach (Ext: $\alpha = 0.25$).

Comparison of error estimators for the cracked plate problem

Several numerical results have been obtained for the gradient recovery approach. Recovery of the tangential derivatives of the various densities is performed, and the individual contributions for the error are combined, with scaling given by Eq. 15. Also, several numerical results are obtained for the external domain error estimator, as the parameter α is varied. In this work, five values of this parameter are tested: $\alpha = 0.01, 0.25, 0.5, 0.75$ and 1.0 . The average of the element errors for each case gives an estimate of global error associated with a particular discretization. Also, this average is used to normalize the element errors to facilitate their comparison.

Figure 2(b) shows the behavior of the average (global) error estimators using gradient recovery (GR:D+T), for the various meshes tested. The behavior for the errors from the external domain approach (Ext: $\alpha = 0.25$) is similar and not shown. In all cases the global error, as estimated by the average of the element errors, decreases with mesh refinement, showing the consistency of the error estimators. We note in Fig. 2(b) that, for this case, the decrease in average error significantly is greater when r -refining than when h -refining the mesh of 78 elements. The error estimators were useful to compare the efficiency of two different types of mesh refinement for this particular problem.

Two different stresses at the exterior evaluation point were defined in Section 3 as estimators for the external domain approach. Figure 3(a) shows the average (global) stress error estimators for the external domain (Ext) approach. This figure compares the influence of the individual contributions of the octahedral stress error (T) and of the mean stress error (M) on the total stress error (T+M) for various values of α . We note from Fig. 3(a) that for $\alpha = 0.25$, the contribution of the octahedral stress is dominant, between 80% and 90% of the total stress error. If $\alpha = 0.25$ is adopted, a simpler error estimator for the external domain approach could be obtained with the evaluation of the octahedral stress only, because the relative contribution of the mean stress to the total error is small, in this case. However, if the contribution of the mean stress to the total error is desired, then other values of α , say, between 0.25 and 0.75, can be considered for a particular problem.

The external error estimators, after being normalized by their average, are now compared for various distances from the exterior point to the boundary. Figure 3(b) shows the influence of the position of the external point for the initial mesh with 78 elements. The error results are plotted for various values of α . The horizontal axis of the various plots corresponds to the s - coordinate of the middle of each element along the boundary, starting from the origin at point B (see Fig. 1(a)). The coordinate of the crack tip O is $s = 51$. The coordinates of the corner nodes B, C, D and A are $s = 0$ (and 60), 20, 30 and 50, respectively.

The high values of the error in the elements in a vicinity of the singular point O are apparent for all values of α . The case of $\alpha = 0.01$ represents an external point very close to the boundary and apparently the numerical errors are mostly associated with the

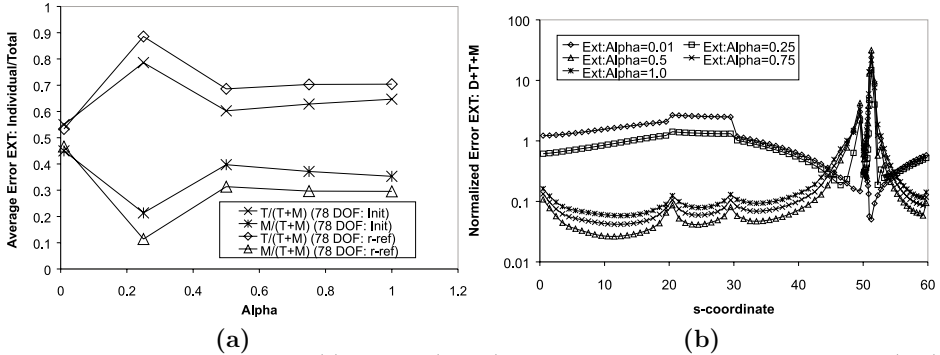


Figure 3: Cracked plate problem: (a) Average (global) error estimators for the external domain (Ext) approach. Influence of the individual contributions of the octahedral stress error (T) and of the mean stress error (M) into the total stress error (T+M) for the various values of α . Plotted error results for various meshes. (b) Influence of the position of the external point for the initial mesh with 78 elements. Plotted error results for various values of α .

near-singularity of the integral equation evaluated at these points. As the distance from the boundary increases, local information on the boundary error become apparent, with the highest relative differences between element errors attained for $\alpha = 0.5$. Error peaks in the vicinity of the various corner nodes are also evident. As α continues to increase, the element differences become smaller, the local information becoming attenuated. When α increases, the information starts losing its local character.

The external error estimator is based on a combination of displacement and stress errors. Figure 4(a) shows the influence of the individual contributions of displacement only (Ext:D), octahedral stress only (Ext:T) and mean stress only (Ext:M) on the total (Ext:D+T+M) error estimator. The initial mesh contained 78 elements, and $\alpha = 0.25$. Clearly, the contribution of the octahedral stress is dominant. The total error curve is very close to the curve obtained with the octahedral stress. The relative dominance of the octahedral stress over the mean stress, for $\alpha = 0.25$, was already noted on Fig. 3(a) for the global errors. But only the mean stress shows clearly the presence of corner nodes, by presenting sudden changes in the error distribution at these corners. The choice of a different value of α , say, between 0.25 and 0.75, will allow for this contribution of the mean stress to be accounted for in the total external error.

Figure 4(b) shows the influence of the individual contributions of the displacements u and v only (GR:u and GR:v) and of the tractions SG and TAU only (GR:SG and GR:TAU) for the gradient recovery (GR:D+T) error estimator. The initial mesh contained 78 elements. The error from the traction TAU only (GR:TAU) is zero everywhere due to boundary conditions. On the side AB , both the individual contributions of the non-prescribed displacement on OB (GR:u only) and of the non-prescribed normal trac-

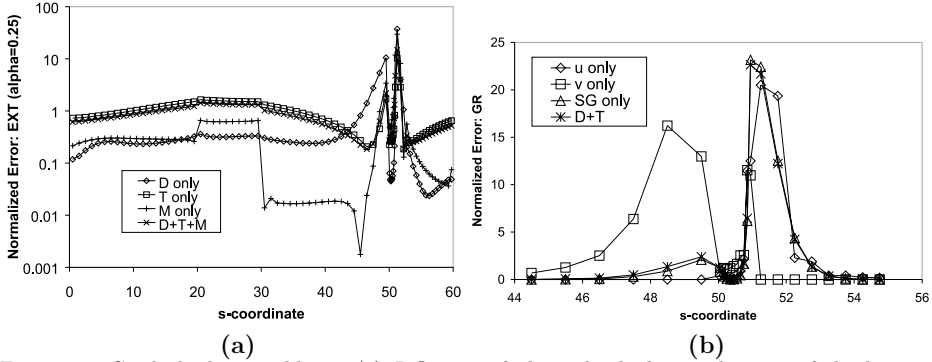


Figure 4: Cracked plate problem: (a) Influence of the individual contributions of displacement only (Ext:D), octahedral stress only (Ext:T) and mean stress only (Ext:M) for the external domain (Ext:D+T+M) error estimator for the initial mesh with 78 elements. (b) Influence of the individual contributions of displacements u and v only (GR:u and GR:v) and traction SG (GR:SG) for the Gradient Recovery (GR:D+T) error estimator for the initial mesh with 78 elements. The error from the traction TAU only (GR:TAU) is zero everywhere due to the boundary conditions. GR:TAU is not plotted herein.

tion on AO (GR:SG only) for the error estimator highlight the high errors in the region near the singular point. The error from the displacement dominates on the elements belonging to the side OB and the error from the traction dominates on the elements belonging to the side AO . On side DA , we note increasing values of the local error in both the non-prescribed displacement (GR:v only) and in the non-prescribed normal traction (GR:SG only) as point A is approached. The non-prescribed density that contains the error information is different in each boundary region, depending on the boundary conditions, and only the total error (GR:D+T) is able to recover the appropriate element error information for all segments of the boundary. Also, due to high errors in the vicinity of the singular point, corner errors are not apparent in this non-log plot.

Figure 5(a) presents a comparison between gradient recovery (GR:D+T) and external (Ext:D+T+M, $\alpha = 0.25$) error estimators for the initial mesh with 78 elements. As expected, both error estimators indicate the same region about the singular point O as having the highest values of error. The corner nodes are more apparent with the gradient recovery than with the external error estimator. This behavior can be explained by the choice of $\alpha = 0.25$ for the external error estimator. As shown in Fig. 3(b), other choices, such as $\alpha = 0.5$, may allow for a better representation of these corner nodes with the external error estimator.

Figure 5(b) shows the influence of mesh refinement for the gradient recovery error estimator with displacements and tractions combined (GR:D+T). Similarly, Fig. 6(a) shows the influence of mesh refinement for the external domain (Ext:D+T+M) error

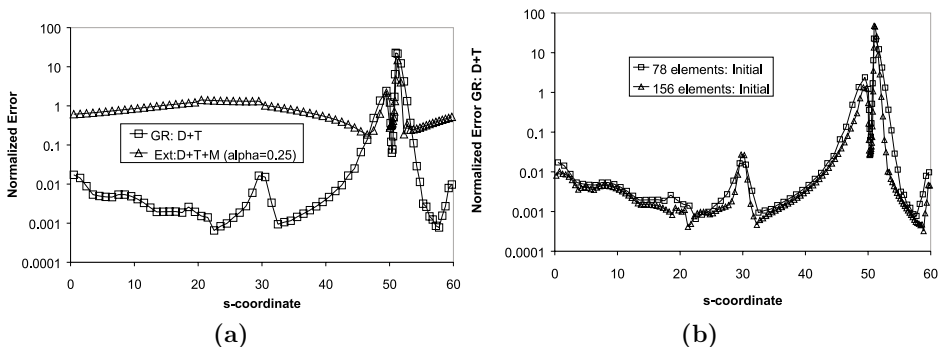


Figure 5: Cracked plate problem: (a) Comparison between Gradient Recovery (GR:D+T) and External (Ext:D+T+M, $\alpha = 0.25$) error estimators for the initial mesh with 78 elements. (b) Influence of mesh refinement for the Gradient Recovery error estimator with displacements and tractions combined (GR:D+T). h -refinement performed on initial mesh of 78 elements.

estimator with $\alpha = 0.25$. In both cases, h -refinement is performed on the initial mesh of 78 elements. These results are qualitatively comparable and consistent as the mesh is refined.

Figure 6(b) shows the influence of r -refinement for the gradient recovery error estimator with displacements and tractions combined (GR:D+T). Similarly, Fig. 7(a) shows the influence of r -refinement for the external domain (Ext:D+T+M) error estimator with $\alpha = 0.25$. In both cases, the r -refinement is performed on the initial mesh of 78 elements by concentrating small elements near the crack tip. Both figures show that the adopted r -refinement procedure redistributes and equalizes errors. The general idea of equalizing the errors on the entire boundary appears clearly in Figures 6(b) and 7(a), where the errors in the vicinity of the crack tip are attenuated.

On the other hand, for the gradient recovery error estimator, the redistribution of the errors shown in Fig. 6(b) leads to an equalization of the element errors on almost all the boundary regions, except for the region near the crack tip, where the errors remain high. The reason for this behavior is that as the elements near the crack tip become smaller, the tangential derivatives become functions with increasingly high slopes, so that the recovery procedure is accounting for increasingly large differences between smoothed and non-smoothed quantities. The gradient recovery error estimator highlights the fact that the error is becoming more localized near the crack tip. The error in the small near-crack-tip element is not decreasing with mesh refinement. Changes other than mesh refinement are needed for the local error near the crack tip to decrease. For example, by substituting the standard Lagrangian near-crack-tip element by a special singular element, the local error in this element is expected to become small.

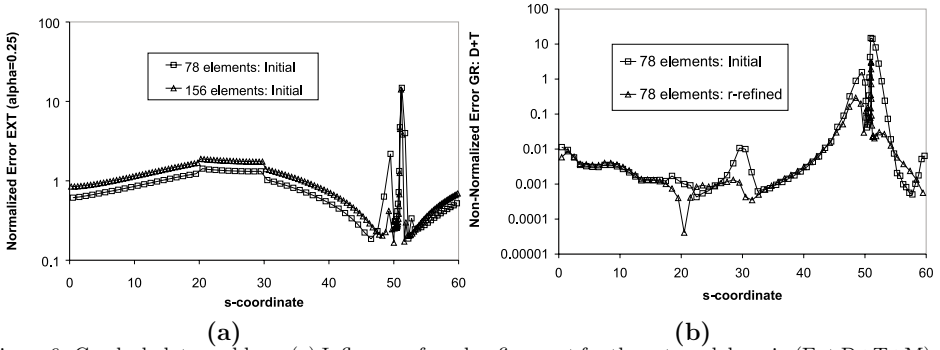


Figure 6: Cracked plate problem: (a) Influence of mesh refinement for the external domain (Ext:D+T+M) error estimator with $\alpha = 0.25$. h-refinement performed on initial mesh of 78 elements. (b) Influence of r -refinement for the Gradient Recovery error estimator with displacements and tractions combined (GR:D+T). r -refinement performed on initial mesh of 78 elements by concentrating small elements near the crack tip.

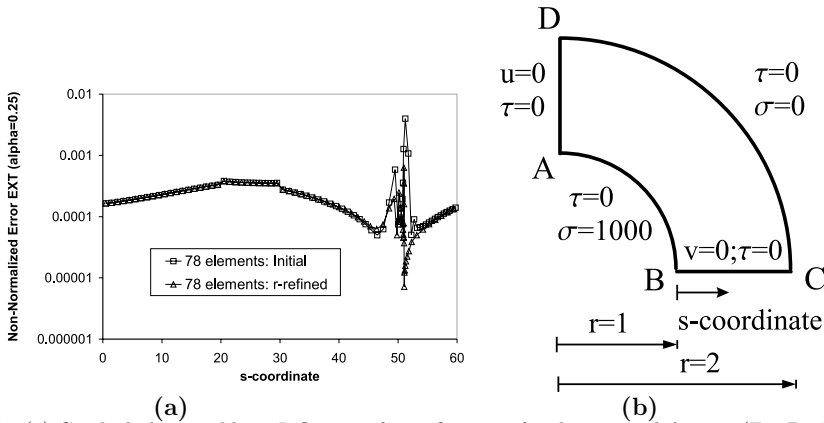


Figure 7: (a) Cracked plate problem: Influence of r -refinement for the external domain (Ext:D+T+M) error estimator with $\alpha = 0.25$. r -refinement performed on initial mesh of 78 elements by concentrating small elements near the crack tip. (b) Axisymmetric pressurized pipe. One-quarter of the pipe cross section is modeled.

4.2 The pipe problem

This example illustrates the use of the two error estimators for an axisymmetric pressurized pipe. Due to symmetry, only one-quarter of the pipe cross section is modeled. Figure 7(b) shows the problem geometry and boundary conditions. The elastic modulus is $E = 3.0 \times 10^7$ units and Poisson's ratio is $\nu = 0.3$.

Several meshes were constructed to evaluate the error estimators for this problem. Figure 8(a) shows the coarsest mesh with 48 elements (96 DOF). Finer meshes with 96 and 192 elements are obtained subsequently by dividing each element by two in each mesh refinement step.

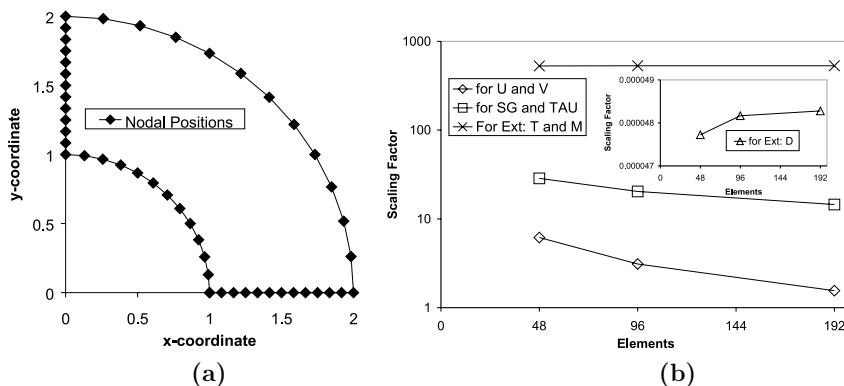


Figure 8: Pipe problem. (a) Coarsest mesh: 48 elements. (b) Scaling factors for the Gradient Recovery (GR:D+T) and for the external domain (Ext:D+T+M) error estimators. Individual contributions of the displacements (u and v) only and of the tractions (SG and TAU) only are scaled before combined to give the GR:D+T error estimator. Similarly, individual contributions of the displacements (D) only and of the invariant stresses (T and M) only are scaled before combined to give the Ext:D+T+M error estimator.

Comparison of the error estimators results for the pipe problem

After the boundary solution is obtained using the BEM code, the local element error is calculated using both the gradient recovery and the external domain approaches. Several numerical results for element error are obtained for the gradient recovery approach, with scaling given by Eq. 15. Figure 8(b) shows the scaling factors for the gradient recovery (GR:D+T) and for the external domain (Ext:D+T+M) error estimators. Individual contributions of the displacements (u and v) only and of the tractions (SG and TAU) only are scaled before combining to give the GR:D+T error estimator. Similarly, individual contributions of the displacements (D) only and of the invariant stresses (T and M) only are scaled before combining to give the Ext:D+T+M error estimator.

Also, several numerical results are obtained for the external domain error estimator, as the parameter α , which gives the distance from the external point to the nearest boundary element, assumes the values: $\alpha = 0.01, 0.25, 0.5, 0.75$ and 1.0 .

Figure 9(a) shows the average (global) error estimators for the gradient recovery (GR) procedure and for the external domain (Ext) approach for various values of α . The average of the element errors for each case gives an estimate of the global error associated with a particular discretization. Also, this average is used to normalize the element errors for their comparison. In almost all cases, the global error, as estimated by the average of the element errors, decreases with mesh refinement, i.e., with increasing number of degrees of freedom (DOF), showing the consistency of the error estimators. The only exception is the external error Ext:D+T+M for $\alpha = 0.01$ where the quasi-singularities due to the location of the external point very near the boundary play a major role in the average error behavior, which is practically constant with mesh refinement.

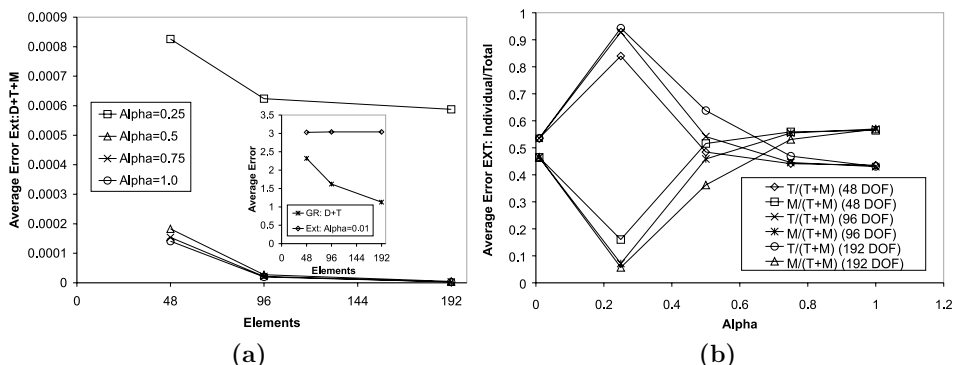


Figure 9: Pipe problem: (a) Average (global) error estimators for the Gradient recovery (GR) procedure and for the external domain (Ext) approach for various values of α . (b) Average (global) error estimators for the external domain (Ext) approach. Influence of the individual contributions of the octahedral stress error (T) and of the mean stress error (M) into the total stress error (T+M) for the various values of α . Plotted error results for various meshes.

Figure 9(b) shows the average (global) error estimators for the external domain (Ext) approach. This figure compares the influence of the individual contributions of the octahedral stress error (T) and of the mean stress error (M) into the total stress error (T+M) for the various values of α . The error results were plotted for the various meshes. Similar to the crack problem, the contribution of the octahedral stress to the total stress error is clearly dominant for $\alpha = 0.25$.

Local normalized external error estimators have been compared for various distances from the exterior point to the boundary. Figure 10(a) illustrates the influence of the position of the external point for the 48-element mesh. The error results were plotted for the various values of α . The origin of the s - coordinate is point B (see Fig. 7(b)). The

coordinates of the corner nodes B , C , D and A are $s = 0$ (and 6.71), 1.0, 4.14 and 5.14, respectively.

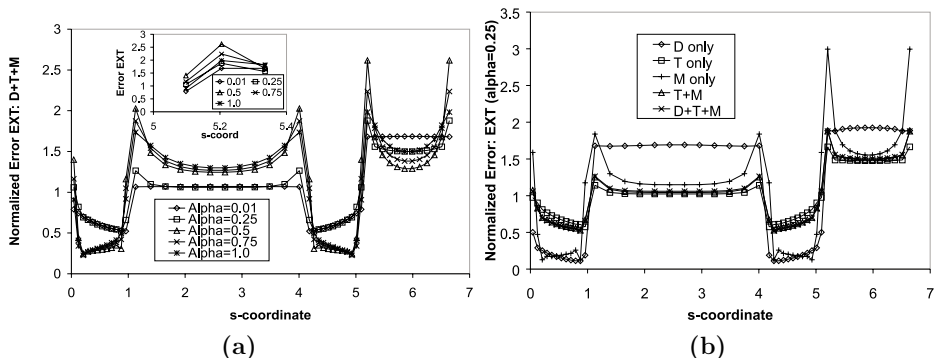


Figure 10: Pipe problem: (a) Influence of the position of the external point for the 48-element mesh. Plotted error results for various values of α . Insert shows errors in region about corner A . (b) Influence of the individual contributions of displacement only (Ext:D), octahedral stress only (Ext:T) and mean stress only (Ext:M) for the external domain (Ext:D+T+M) error estimator for the 48-element mesh.

The error results for $\alpha = 0.01$ present the least variation of all cases. This case represents an external point very near the boundary, with numerical errors primarily associated with near-singularities of the integral equation. When the value of α increases from 0.01 to 0.5, the relative differences in the element errors increase, so that qualitative comparisons for the local error can be made. But when α continues to increase, the local information becomes attenuated. This phenomenon can be clearly seen, for example, for the elements near corner nodes. The inset in Fig. 10(a) shows the errors in a region about corner node A . When α increases, the information on the error begins to lose its local character.

Figure 10(b) shows the influence of the individual contributions of displacement only (Ext:D), octahedral stress only (Ext:T) and mean stress only (Ext:M) for the external domain (Ext:D+T+M) error estimator for the 48-element mesh. Similar to the crack problem, the contribution of the mean stress clearly identifies the error at the corner nodes.

Figure 11(a) shows the influence of the individual contributions of the displacements u and v only (GR: u and GR: v) and of the tractions SG and TAU only (GR:SG and GR:TAU) for the gradient recovery (GR:D+T) error estimator for the 48-element mesh. The error from the traction TAU only (GR:TAU) is zero everywhere due to the boundary conditions. Similar to the crack problem, the individual contributions were able to identify errors in regions where the respective density was not prescribed. Only the total error (GR:D+T)

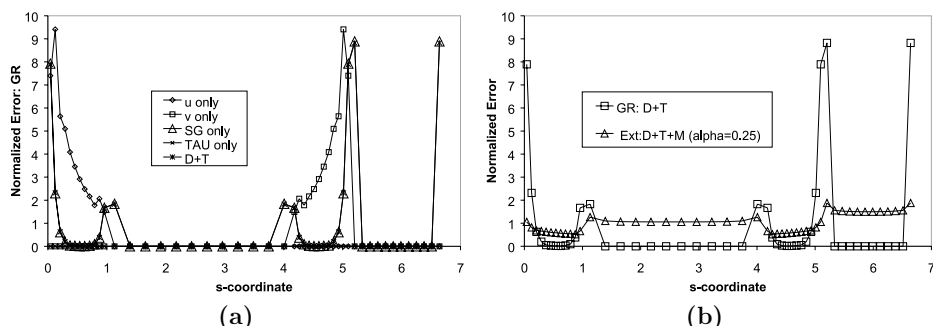


Figure 11: Pipe problem: (a) Influence of the individual contributions of displacements u and v only (GR: u and GR: v) and tractions SG and TAU only (GR:SG and GR:TAU) for the Gradient Recovery (GR:D+T) error estimator for the 48-element mesh. The error from the traction TAU only (GR:TAU) is zero everywhere due to the boundary conditions. (b) Comparison between Gradient Recovery (GR:D+T) and External (Ext:D+T+M, $\alpha = 0.25$) error estimators for the 48-element mesh.

is able to show consistent error information in all boundary segments, regardless of the boundary conditions.

Figure 11(b) presents a comparison between gradient recovery (GR:D+T) and external (Ext:D+T+M, $\alpha = 0.25$) error estimators for the 48-element mesh. Both error estimators exhibit similar qualitative behavior in the vicinity of the corner nodes. Similar to the crack problem, the large external errors at corner nodes are more attenuated for $\alpha = 0.25$ than, for example, for $\alpha = 0.5$, as shown in Fig. 10(a). This result can be explained from the fact that the contribution of the mean stress to the external error is less important for $\alpha = 0.25$, as shown in Fig. 9(b), and the mean stress was shown in Fig. 10(b) to be the error component that better indicates the external error at the corner nodes.

Figure 12(a) shows the influence of mesh refinement for the gradient recovery error estimator with displacements and tractions combined (GR:D+T). Similarly, Fig. 12(b) shows the influence of mesh refinement for the external domain (Ext:D+T+M) error estimator with $\alpha = 0.25$. All these error results are qualitatively comparable and consistent with mesh refinement.

5 CONCLUSIONS

Error estimators based on gradient recovery and external solution show consistency with mesh refinement and give similar qualitative results. The error estimators were also proven to be useful to compare the efficiency of two different types of mesh refinement (r - and h -refinement) for a particular problem.

The error estimator using the gradient recovery approach presents a more general characteristic as this formulation does not rely on an “optimal” choice of an external

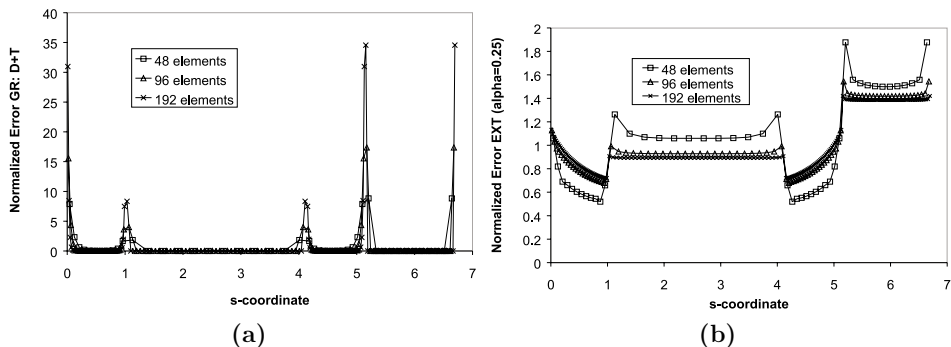


Figure 12: Pipe problem: (a) Influence of mesh refinement for the Gradient Recovery error estimator with displacements and tractions combined (GR:D+T). (b) Influence of mesh refinement for the external domain (Ext:D+T+M) error estimator with $\alpha = 0.25$.

parameter, such as in the case of the external domain error estimator. Also, the external domain error estimator can be used only for domains in which an exterior region exists, while the gradient recovery approach can be used on a broader range of elastostatics problems.

The external error results for $\alpha = 0.01$ present the least variation of all cases, which can be explained by the fact that the element errors are dominated by the near-singular behavior of the integrals, and not by the discretization error. As the distance from the boundary increases, local information becomes more apparent. The highest relative differences between element errors and the highest error peaks in the vicinity of the various corner nodes were attained for $\alpha = 0.5$. When α increases further, the information begins to lose its local character.

The relative contributions of the octahedral and mean stresses to the total external error is dependent on the choice of the external point. The octahedral stress is dominant over the mean stress for $\alpha = 0.25$. Also, the external errors at the corner nodes are more attenuated for $\alpha = 0.25$ than, for example, for $\alpha = 0.5$. The mean stress is the error component that better indicates the external error at the corner nodes. Choices of values of α between 0.25 and 0.75 allow for the contribution of the mean stress to be accounted for adequately in the total external error.

The individual contributions to the gradient recovery error estimator were able to identify errors only in the regions where the respective density was not prescribed. Only the total error (GR:D+T) was able to report consistent error information on all boundary segments, regardless of the boundary conditions.

The gradient recovery and the external error estimators exhibit similar behavior in the vicinity of the corner nodes, although the various corner nodes were found to be more evident with the gradient recovery approach than with the external error estimator.

Importantly, both error estimators indicate the same region about the singular point as having the highest values for the normalized error.

The redistribution of the error with r -refinement leads to an equalization of the element errors on almost all the boundary regions, except for the region near the crack tip, where high errors remained. The gradient recovery error estimator highlights the fact that as the error becomes more localized near the crack tip, the error in the small near-crack-tip element does not decrease, even with the mesh refinement.

The replacement of the standard near-crack-tip element by a special singular element is expected to improve these local error results.

Future work on this topic could include the extension of the two error estimators for higher order elements, for 2-D potential and elastostatics problems.

Acknowledgments

The first two authors acknowledge the support received from CNPq - Conselho Nacional de Desenvolvimento Científico e Tecnológico and from FAPEMIG - Fundação de Amparo à Pesquisa do Estado de Minas Gerais. The third author gratefully acknowledges support by the National Science Foundation (CTS-9983961).

REFERENCES

- [1] A. B. Jorge, G. O. Ribeiro and T. S. Fisher: New Approaches for Error Estimation and Adaptivity for 2-D Potential Boundary Element Methods, *Int. J. Numer. Meth. Engrg.*, accepted for publication, 2002.
- [2] S. Liapis: A review of error estimation and adaptivity in the boundary element method, *Eng. Anal. Bound. Elem.*, 14, pp. 315–323, 1994.
- [3] E. Kita and N. Kamiya: Recent studies on adaptive boundary-element methods, *Adv. Eng. Softw.*, 19, pp. 21–32, 1994.
- [4] E. Kita and N. Kamiya: Error estimation and adaptive mesh refinement in boundary element method, an overview, *Eng. Anal. Bound. Elem.*, 25, pp. 479–495, 2001.
- [5] M. A. Ainsworth, & J. T. Oden: A posteriori error estimation in finite element analysis, *Comput. Methods Appl. Engrg.*, 142, pp 1-88, 1997
- [6] M. Denda and Y. F. Dong: An error estimation measure in the direct BEM formulation by the external Somigliana's identity, *Comput. Methods Appl. Mech. Engrg.*, 173, pp. 433–447, 1999.
- [7] F. Paris and J. Cañas: *Boundary Element Method - Fundamentals and Applications*, Oxford Univ. Press, New York, 1997.
- [8] T. A. Cruse: *Boundary Element Analysis in Computational Fracture Mechanics*, Kluwer Academic Publishers, Norwell, Massachusetts, 1988
- [9] W. H. Press, S. A. Teukolsky, W. T. Vetterling and B. P. Flannery, *Numerical recipes in FORTRAN - The art of scientific computing*, 2nd Ed., Cambridge University Press, 1992